Int. J. Nonlinear Anal. Appl. 14 (2023) 6, 73–83
ISSN: 2008-6822 (electronic)
http://dx.doi.org/10.22075/ijnaa.2022.28490.3916

Optimal position control of shape memory alloys actuator with nonlinear behavior by using states dependent Riccati equation (SDRE)

Alireza Naeimifard*, Afshin Ghanbarzadeh, Valid Alimaleki

Department of Mechanical Engineering, Shahid Chamran University of Ahvaz, Ahvaz, Iran

(Communicated by Seyyed Mohammad Reza Hashemi)

Abstract

Several studies have been conducted to accurately control the deformation of Shape Memory Alloys (SMAs) as an actuator, however, due to the non-linear relationship between the change of mechanical structure, including stress and strain, they have often been associated with a challenge. In the current study, a wire made of intelligent memory alloy (Nitinol) is used as an actuator of one degree-of-freedom mechanism. In order to observe the operation of the wire under electrical stimuli, a laboratory set-up is implemented. Our main goal is to accurately control the position of this nonlinear system with high precision by using optimal control. So, the nonlinear system equations are extracted and sorted into state-dependent matrices and the State-Dependent Riccati Equation (SDRE) is used to find the optimal control value. To verify the experiment three inputs including multiple steps, a low-frequency sine wave and a high-frequency sine wave, are applied to the system. The results, show the good performance of the controller in sustainability, fast response, and tracking of the desired position with low overshoot.

Keywords: Nonlinear control, Optimal control, Smart material, Shape memory alloys, States dependent riccati equation
2022 MSC: 58E25, 70E60

1 Introduction

Shape memory alloys are a group of smart memory materials that have the ability to return to their previous shape if exposed to thermal and magnetic stimuli. The unique properties of shape memory alloys were not well known until 1962 when William Behler and Frederick Wang demonstrated the shape memory effect in a nickel-titanium alloy (nitinol).

The combination of their high stiffness, high strength, and large recovery strain offers great potential for the use of SMAs as actuators in diverse applications. These include aircraft wing shape control, automotive, aerospace, microrobot manipulation, active endoscopy, prosthetic end-effector actuator, micro rotary actuator, micro fiber switch, micro-electromechanical connectors, smart structures and composites [13].

*Corresponding author
Email addresses: naeimifard.a@scu.ac.ir (Alireza Naeimifard), ghanbarzadeh.a@scu.ac.ir (Afshin Ghanbarzadeh), valimaleki74@gmail.com (Valid Alimaleki)

Received: June 2022 *Accepted:* September 2022

The main challenge in the position controlling of shape memory alloys is its non-linearity behavior due to the hysteresis effect and residual stress during the process of heating and cooling in them. Several methods are proposed to control the exact position of actuators made of shape memory alloys, including non-linear methods and pulse width modulation [20]. Elahinia and Ashrafion [6] used the variable structure controller to control the mechanism of one degree of freedom with a memory alloy wire driver. The pulse width modulation is used to implement the proportional-derivative controller to stimulate the nitinol wire [11]. Also, in another study the self-tuning fuzzy PID base controller in which the system parameters were tuned by the fuzzy algorithms is implemented to control the SMA actuator [8]. In the same relevant ones is offered for position control of SMAs [17].

Considering the advantage of state variable dependent Riccati equation (SDRE) technique in feedback controller problems as well as non-linear optimal control problems is main reason for which growing rapidly. One of the most important advantages of optimal control with the help of Riccati equation dependent on state variables is the possibility of achieving robust control criteria and minimum output error in SMAs base actuators [14, 15, 10]. In the other study a control algorithm is proposed in which using the inverse hysteresis along with an artificial neural network of radial basis functions to compensates the feedback [1].

Most of the SMA actuator applications mentioned earlier in this section use SMA wires, because they are easy to cut, to connect, and to activate electrically. It is common to obtain an inelastic strain in phase by virtue of a bias spring is connected in series with the SMA wire. Thus, the wire contracts when heated, and it expands with the aid of the bias spring when cooled. A schematic of a spring-biased SMA wire actuator and the experimental setup are shown in Fig. 1. In this paper, we propose a complete mathematical model of this spring-biased SMA wire actuator. This paper uses experimental results obtained by Ma et al. [11] on their experimental setup for spring-biased SMA wire actuator.

2 Method, materials and equipment

In this research, the accurate control of the position or change of the length of the memory wire. For this purpose, a mechanism including a spring and a memory alloy wire has been used. Figure 1 shows a simple picture for a better understanding of this issue. As seen in Figure 1, this equipment includes a nitinol memory alloy wire, rotary encoder, pole, spring, Arduino board and direct current generator. The used wire has a diameter of 5.0 mm and austenite transformation temperature of $55°C$. This wire was purchased from Lint Steels and has 45% titanium and 55% nickel. The used rotary encoder has an accuracy of one tenth of a degree. This encoder is used as a sensor to measure the length of the wire. The pulley mounted on the encoder has two centimeters diameter. A spring is used to supply initial tension and stretch the wire. Arduino mega board is used to read the number of encoder pulses and convert them into digital data. Finally, a direct current generator is used to apply current to the wire. To apply the current calculated by MATLAB software to the SMAs wire, a driver named L293 is used. Also, the parameters required in the modeling based on the properties of the wire used in the laboratory equipment are according to Table (2)2, in which some of them were obtained by trial and error.

One of the important advantages of SDRE optimal control is the possibility of achieving robust control criteria and minimum output error in memory operators [1]. In this research, the optimal control method using the Riccati equation depending on the state variables is placed in the category of non-linear controllers. To minimize the objective function, the appropriate selection of weight matrices Q and R is very important in the speed and accuracy of optimization [2]. Therefore, the response of the actuated system of the setup under different weighting matrices have been measured and saved to compare them together.

3 SDRE Method

Consider the continuous-time, autonomous, affine nonlinear system which has dynamics

$$\dot{x} = f(x) + G(x)u, x(0) = x_0 \tag{1}$$

with state vector $x \in R_n$, control vector $u \in R_m$, $f(x) \in R_n, f(x) \in R_{n\times m}$, ϵ and $g(x) \neq 0$ for any x. The control objective is to design control law u which can minimize the following non-quadratic performance index:

$$I = \int_{t_0}^{t_f} x^T(t)Q(x)x(t) + u^T(t)R(x)u(t)dt \tag{2}$$

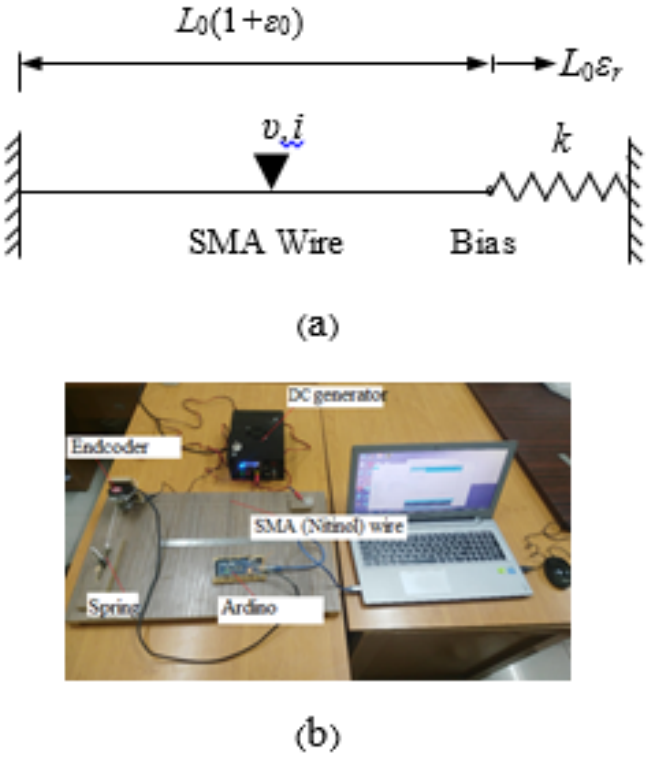

Figure 1: a) Simple Scheme of SMAs experiment, b) SMA wire test benches setup

where, $Q(x)$ is the state weighting matrix which is semi-positive definite, $Q(x) \in R^{n\times n}$. $R(x)$ is the control weighting matrix which is positive definite, $R(x) \in R^{m\times m}$. $Q(x)$ and R(x) can be constant or state-dependent. According to optimal control theory, the optimal control problem described by (1)-(2) can be resolved by Hamilton-Jacobi-Bellman (HJB) partial differential equation:

$$\frac{\partial V^T}{\partial x} f(x) + \frac{1}{2} x^T Q(x) x - \frac{1}{2} \frac{\partial V^T}{\partial x} g(x) R(x)^{-1} g(x)^T \frac{\partial V^T}{\partial x} = 0 \tag{3}$$

with

$$V(x) = min_u \frac{1}{2} \int_0^\infty x^T(t) Q(x) x(t) + u^T(t) R(x) u(t) dt \tag{4}$$

where $V(x)$ is supposed to be continuous differentiable with $V(x) > 0, V(0) = 0$, such that the optimal control law is:

$$u(t) = -R^{(-1)}(x) g^T(x) \frac{\partial V}{\partial x} \tag{5}$$

But it's difficult to solve HJB equation, so that it has difficulty in project application. SDRE method is adopted in this paper to transform the problem of HJB into the problem of solving state-dependent Riccati equation. For autonomous and affine nonlinear system given by (1), the origin of state space is the system equilibrium point, $f(x)$ is continuous differentiable with $f(0) = 0$, (1) can be rewritten in state-dependent coefficient (SDC) form,

$$\dot{x} = A(x)x + B(x)u \tag{6}$$

The matrices $A(x)$ and $B(x)$ should be such that the system is controllable and observable for all the values of the state variables [18, 7].

Then optimal control problem described by (1)-(2) can be transformed into solving SDRE,

$$A^T(x)P(x) + P(x)A(x) + Q(x) - P(x)B(x)R^{-1}(x)B^T(x)P(x) = 0 \tag{7}$$

and the optimal control law is obtained in the form:

$$u(t) = -R^{(-1)}(x)B^T(x)P(x)x = K(x)x \tag{8}$$

where $P(x)$ is the unique, symmetric and positive-definite solution of state-dependent Riccati equation (7).

The method of applying optimal control is that first the so-called quasi-linear form or the linear form developed from the non-linear system is calculated with the help of equation (6). It is assumed that the nonlinear system will behave as an order of time invariant nonlinear system [15]. Then the optimal value of the Riccati equation is obtained in each time step. Therefore, the algebraic Riccati equation must be calculated and solved at each time step using the state-dependent Riccati equation that can be seen in equation (3). The schematic of this process can be seen in Figure 2.

In this research, the state feedback closed loop system along with an integrator is used to optimally track the reference input. The equations of the closed loop system are finally defined as follows with the presence of this integrator:

$$\begin{cases} \begin{bmatrix} \dot{x} \\ \dot{e_i} \end{bmatrix} = \begin{bmatrix} A(x) - B(x)K_1 & -B(x)K_2 \\ DK_1 - C & DK_2 \end{bmatrix} \begin{bmatrix} x \\ e_i \end{bmatrix} + \begin{bmatrix} 0 \\ 1 \end{bmatrix} r \\ y = \begin{bmatrix} C - DK_1 & -DK_2 \end{bmatrix} \begin{bmatrix} x \\ e_i \end{bmatrix} \end{cases} \tag{9}$$

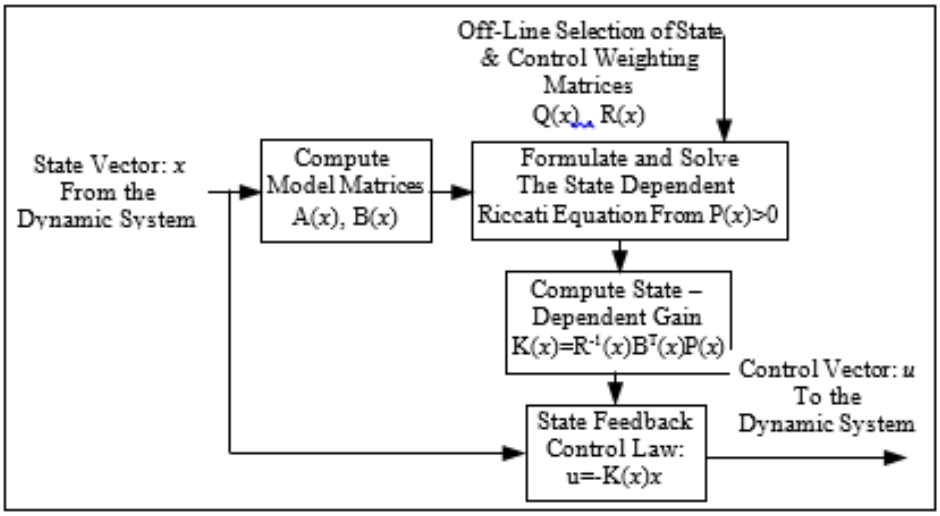

Figure 2: Optimal control diagram of SDRE

4 Heat transfer modeling

The desired system receives its thermal energy from electrical current to heat up the SMAs. The thermal energy balance dictates the temperature of the memory alloy wire where a part of generated heat should be transferred to the environment. It has been assumed that the internal resistance of the wire for conductive heat transfer is negligible against displacement heat transfer to the environment [5]. This assumption is valid for heat transfer inside metal samples [4]. In the end, the temperature T of the memory alloy wire will be obtained using the conduction heat transfer equation (10) [16].

$$\begin{aligned} m\dot{c}\Delta T &= Q_i n - Ah(T - T_0) \\ \rho c(\pi d_0^2 L_0)/4dT/dt &= Ri^2 - \pi d_0 L_0 h(T - T_0) \end{aligned} \tag{10}$$

where ρ is the mass density of the buffered alloy wire, c is the specific heat of the SMAs wire, d_0 is the diameter of the wire in the initial state, L0 is the initial length of the memory alloy wire, h is the convection heat transfer coefficient, i is the electric current inside and T_0 is the temperature of the surrounding environment.

In some literature the convection heat transfer coefficient h and specific heat c should be changed with respect to the SMAs temperature, and should be evaluated by equations (11) and (12) [5].

$$h = \begin{cases} a_1 - a_2 T & \dot{T} \geq 0 \\ a_3 + a_4 \ erf\left(\dfrac{T - m_1}{n_1}\right) & \dot{T} < 0 \end{cases} \tag{11}$$

$$c = b_1 + b_2 \ erf\left(\frac{T - m_2}{n_2}\right) \tag{12}$$

where $a_1, a_2, a_3, a_4, b_1, b_2, m_1, m_2, n_1$ and n_2 are constant parameters.

5 Martensite-temperature residual fraction model

Austenite-martensite transformation in memory alloy materials has residual behavior. As a result, the relationship between the martensite fraction R_m and the temperature T will show a residual behavior [12]. An example of the relationship between these two are shown in Figure 4. In some researches, it has been stated that the temperature of the beginning and end of transformations will change with applied stress [3]. However, this change is insignificant and can be ignored [5]. Therefore, with an acceptable assumption, M_S, M_f, A_S and A_f, which are respectively the start temperature of martensite transformation, the end temperature of martensite transformation, the start temperature of austenite transformation, and the end temperature of austenite transformation can be assumed to be constant.

Various models were developed to express the hysteresis behavior of memory alloy actuators [19, 18, 7, 9]. In this study, the relationship between martensite fraction Rm and temperature T is expressed as [5].

$$h = \begin{cases} (dR_m)/dT = \begin{cases} (h_-(T) + R_m - 1)/(h_+(T) - h_-(T))g_+(T) & \dot{T} \geq 0 \\ (h_+(T) + R_m - 1)/(h_-(T) + h_+(T))g_-(T) & \dot{T} < 0 \end{cases} \\ R_m(0) = 1 \end{cases} \tag{13}$$

Where;

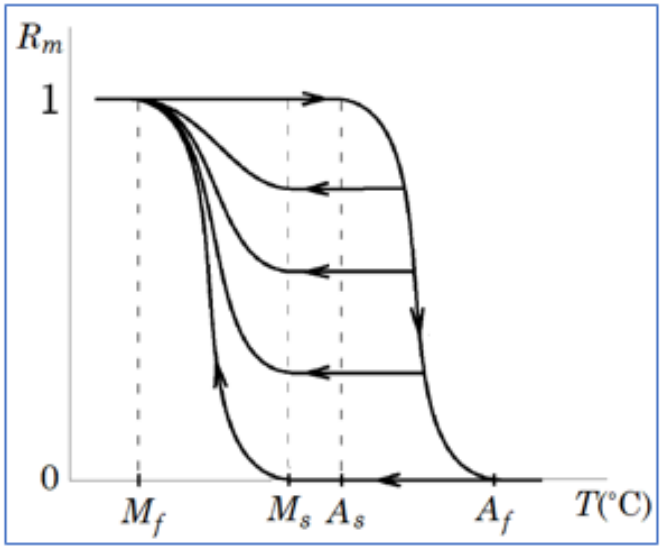

Figure 3: Scheme of SMA residual behavior [5]

$$g_+(u) = 1/(\sigma_+\sqrt{2\pi}) \ ex \ p\left(-(u - u_+)^2/(2\sigma_+^2)\right) \tag{14}$$

$$g_-(u) = 1/(\sigma_-\sqrt{2\pi}) \ ex \ p\left(-(u - u_-)^2/(2\sigma_-^2)\right) \tag{15}$$

Also,

$$h_+(u) = 1/2\left[1 + \ erf\left((u-u_+)/(\sigma_+\sqrt{2})\right)\right] \tag{16}$$

$$h_-(u) = 1/2\left[1 + \ erf\left((u-u_-)/(\sigma_-\sqrt{2})\right)\right] \tag{17}$$

In relations (14) to (17), μ is the mean and σ^2 is the covariance of the residual loops in figure 3.

6 Strain model

The overall strain of the wire depends on factors such as pre-strain or initial strain $\backslash epsilon - \{0\}$, spring stiffness and physical parameters of memory alloy wire materials. However, the approximate relationship between ϵ strain and martensite fraction Rm has been extracted using the MATLAB curve fitting toolbox [5].

$$\epsilon = \epsilon_0 + k_1 R_m + k_2 R_m^2 + k_3 R_m^{50} \tag{18}$$

Where k_1, k_2 and k_3 are constant parameters.

7 Electrical resistance model

In this section, using the variable sub-layer model, the electrical resistance of SMAs wire is modeled as a function of R_m, T and ϵ. The two phases of austenite and martensite should be considered in parallel [5]. The electrical resistance of SMAs wire can be evaluated as:

$$1/R = (\pi d_0^2)/\left(4L_0(1+2\epsilon)\right)\left[(1-R_m)/(\rho_A(T)) + R_m/(\rho_M(T))\right] \tag{19}$$

Where $\rho_M(T)$ and $\rho_A(T)$ are specific electrical resistance of austenite and martensite phase respectively, and

$$\rho_A(T) = p_1 + p_2 \ exp\left(-p_3(T - T_\alpha mb)\right) \tag{20}$$

$$\rho_M(T) = (q_1 - q_2 T)\left[1 + erf\left((T-m_3)/n_3\right)\right] + \sum_{i=0}^{9} \alpha_i (T - T_{amb})^i \tag{21}$$

where $p_1, p_2, p_3, q_1, q_2, m_3, n_3$ and $\alpha_i (i = 1, \ldots, 9)$ are constant. Hence, the state space is developed by considering:

$$h = \begin{cases} x_1 = R_m \\ x_2 = T - T_0 \\ u = i^2 \end{cases} \tag{22}$$

$$\dot{x_1} = a_{11}x_1 + a_{12}x_2 + b_{11}u$$

$$\dot{x_2} = -\frac{4h}{d_0\rho c}x_2 + \frac{4R}{\pi d_0^2 L_0 \rho c}u \tag{23}$$

where,

$$a_{11} = \begin{cases} \left(\dfrac{g_+(T)}{(h_+(T)-h_-(T))}\right)\left(-\dfrac{4h}{d_0\rho c}x_2\right) & \dot{T} \geq 0 \\ \left(\dfrac{g_-(T)}{(h_-(T)+h_+(T))}\right)\left(-\dfrac{4h}{d_0\rho c}x_2\right) & \dot{T} < 0 \end{cases} \tag{24}$$

$$a_{12} = \begin{cases} \left(\dfrac{(h_-(T)-1)g_+(T)}{(h_+(T)-h_-(T))}\right)\left(-\dfrac{4h}{d_0\rho c}\right) & \dot{T} \geq 0 \\ \left(\dfrac{(h_+(T)-1)g_-(T)}{(h_-(T)+h_+(T))}\right)\left(-\dfrac{4h}{d_0\rho c}\right) & \dot{T} < 0 \end{cases} \tag{25}$$

$$b_{11} = \begin{cases} \left(\dfrac{(h_-(T)-1)g_+(T)}{(h_+(T)-h_-(T))} + \dfrac{g_+(T)}{(h_+(T)-h_-(T))}x_1\right)\left(\dfrac{4R}{\pi d_0^2 L_0\rho c}\right) & \dot{T} \geq 0 \\ \left(\dfrac{(h_+(T)-1)g_-(T)}{(h_-(T)-h_+(T))} + \dfrac{g_-(T)}{(h_-(T)-h_+(T))}x_1\right)\left(\dfrac{4R}{\pi d_0^2 L_0\rho c}\right) & \dot{T} < 0 \end{cases} \tag{26}$$

$$y = R_M = x_1, \ or \ C = [0 \ \ 1] \tag{27}$$

Also for equilibrium points:

$$E_0 = (0 \ \ 0) \tag{28}$$

8 Results

Important indicators to evaluate the performance of a controller are usually based on system stability, the time to reach the desired output and the amount of energy consumed by the controller. In this section, by stating the results of the simulation, it has been tried to examine the mentioned cases for the proposed system. In this regard, the desired system has been investigated under multiple step inputs, sine wave with high and low frequencies. Considering that the weight matrices Q and R play an important role in the speed and accuracy in the Riccati equation depending on the state variables. Therefore, in addition to different inputs, at least two different weight matrices have been used to investigate how they affect the controller's performance in the multiple step input. These matrices can be seen in equations (12) and (13).

$$\begin{cases} Q_1 = \begin{bmatrix} 1 & 0 & 0 \\ 0 & 0 & 0 \\ 0 & 0 & 100 \end{bmatrix} \\ R_1 = 0.001 \end{cases} \tag{29}$$

$$\begin{cases} Q_2 = \begin{bmatrix} 1 & 0 & 0 \\ 0 & 0 & 0 \\ 0 & 0 & 40 \end{bmatrix} \\ R_2 = 0.005 \end{cases} \tag{30}$$

In the Q matrix, the values on the diagonal are the weight of the martensite fraction variables, the temperature of the memory alloy wire, and the system error, respectively. Of course, the controller should more attempt to bring system back to the equilibrium point. On the other hand, for the R matrix, the values on the diagonal are the weight of the controlled signal by which larger value the controller will be more cautious in using the control signal. By looking carefully at the weight matrices, it is found that the first set of matrices in Eq. (29) has a lower control weight, so its controller is expected to consume more energy and higher output error. This means that the controller with corresponding weighting matrix will perform better when it comes to the reference tracking.

Figure 4 shows that the performance of system tracking to the reference input for weight matrices Q_1 and R_1. According to the figure, except at the beginning the response of the system has a relatively small jump, its performance in tracking the reference input is acceptable, and by changing it, the system can reach the reference value in less than two seconds. The reduction of overshoot for the next input steps occurs due to the slow cooling process of the memory alloy materials. In the lower part of figure 4 it shows that the system error or difference between the reference output and input at any response time. Also, it is show that except in the initial response time and times when the input is changed, during the last of response time the error approach to zero. Therefore, this can indicate that the controller is successful to track the reference input.

To investigate the effect of weight matrices on the performance of the controller in following the reference input, weight matrices Q2 and R2 have also been used. The result is shown in figure 5. With more precision, it will be clear in two ways that error signal in figure 5 is bigger than that in figure 4. The difference between the error signal in the two figures is insignificant, but this insignificant amount is related to the difference in the weight matrices. The reason why the controller in Figure 4 has less error than in Figure 5 is that, firstly, the selected weight for the total system error variable is higher in the first case than in the second case. This improves the performance of the controller in following the input. Second, in the first case, the controlled input weight is lower than the second case. This allows the first controller to consume more control power. Finally, table 1 has been prepared to compare the amount of mutation produced for two selected matrices.

According to table 1, the lower the weighing controller matrix R, has the better performance in general. But it should be noted that by reducing this controlling weight matrix, the system control signal will be increased. This should be problematic in some systems that have physical limitations. However, by choosing the state dependent weight matrices, it is possible to decrease both of settling time and overshoot to the desired level.

Table 1: Control performance with different weighting matrix

Settling time (s)	Overshoot %	Weighting matrix
4.1	5	Q_1 and R_1
1.2	12	Q_2 and R_2

In some of the reviewed researches, it has been stated that SMAs actuators perform poorly in responding to high frequency input. Therefore, in this research, the reaction of the system to sinusoidal inputs with different frequencies

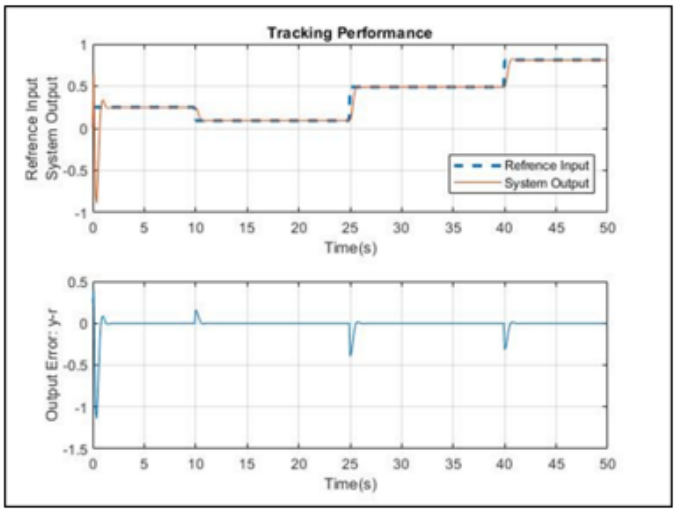

Figure 4: Simulation of system tracking under multi steps input with Q_1 and R_1 weighting matrix

is investigated. The results of the system response to these inputs are shown in figures (6) and (7). Weight matrices Q_1 and R_1 have been used for both inputs.

It can be clearly seen that except for the fluctuations at the beginning of response, the controller has an acceptable performance to tracking the two sinusoidal reference inputs after the first few seconds. Of course, it can be seen in the lower part of figures (12) and (13) that the error is not zero at different times and fluctuates around zero. This is because the system response to the reference input has a delay of less than one second.

9 Conclusion

The optimal control strategy for a class of affine nonlinear systems with hysteresis based on SDRE is proposed in this paper. Thus, SDRE method is implemented to deal with the nonlinear systems controllers, and a way to choose state-dependent weighting matrices $Q(x), R(x)$ is proposed. Also, the simulation is carried out with a SMAs model. It can be seen from the simulation that, SDRE is effective in designing and implementing optimal controller for the SMAs, and with proper state-dependent weighting matrices $Q(x), R(x)$, the system can be driven to equilibrium point quickly. Finally, by using optimal SDRE for tracking case efforts specially in high frequency reference input, the simulation response has a valuable compatibility and low error as shown in Fig. 7. However, an obvious advantage offered by SDRE for controller design is that, it can tradeoff between control efforts and performances by choosing state-dependent weight matrices $R(x), Q(x)$ properly. Consequently, the soft computing method should be used to find the best weighting matrices for great performance.

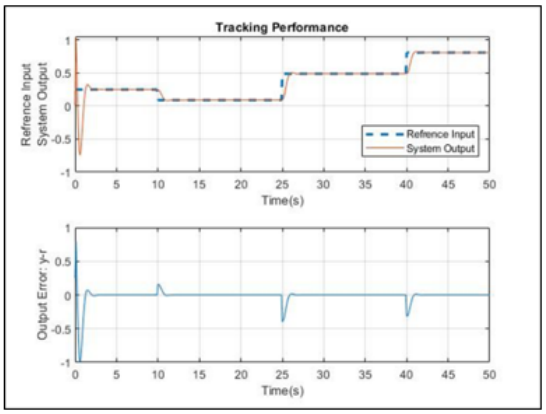

Figure 5: Simulation of system tracking under multi steps input with Q2 and R2 weighting matrix

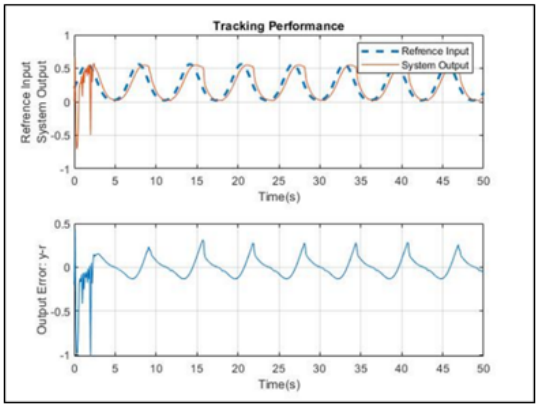

Figure 6: Simulation of system tracking under low frequency input with Q_1 and R_1 weighting matrix

Table 2: Parameters used to simulate the mathematical model of shape memory materials

Parameter	Value	Units	Ref.	Parameter	Value	Units	Ref.
ρ	6500	kgm^{-3}		T_0	24	$^{\circ}C$	
L_0	0.2286	m		d_0	3.814×10^{-4}	m	
a_1	165	$Wm^{-20}C^{-1}$	[11]	b_1	1400	$Jkg^{-10}C^{-1}$	[11]
a_2	0.5	$Wm^{-20}C^{-1}$	[11]	b_2	1000	$Jkg^{-10}C^{-1}$	[11]
a_3	300	$Wm^{-20}C^{-1}$	[11]	m_1	48	$^{\circ}C$	[11]
8 a_4	150	$Wm^{-20}C^{-1}$	[11]	m_2	58	$^{\circ}C$	[11]
n_1	10	$^{\circ}C$	[11]	n_2	0.5	$^{\circ}C$	[11]
μ_+	78.9	$^{\circ}C$	[5]	σ_+	11.2	$^{\circ}C$	[5]
μ_-	34	$^{\circ}C$	[5]	σ_-	5.8	$^{\circ}C$	[5]
Δ	0.04425	m	[5]	k	58.19	Nm^{-1}	[5]
E_a	35917	MPa	[5]	E_m	20480	MPa	[5]
E_T	826	MPa	[5]	E_d	16800	MPa	[5]
ϵ_m^y	0.1		[5]	ϵ_m^d	0.15		[5]
k_1	0.0204		[5]	k_2	0.1293		[5]
k_3	0.0027		[5]				[5]
p_1	9.2×10^{-7}	Ωm	[5]	q_1	3.4×10^{-8}	Ωm	[5]
p_2	8.4×10^{-7}	Ωm	[5]	q_2	9.2×10^{-7}	$\Omega m^{\circ}C^{-1}$	[5]
p_3	8.2499	$^{\circ}C^{-1}$	[5]	m_3	70	$^{\circ}C$	[5]
n_3	30	$^{\circ}C$	[5]				[5]
α_0	8.7×10^{-7}	Ωm	[5]	α_1	4.8×10^{-8}	$\Omega m^{\circ}C^{-1}$	[5]
α_2	-7.8×10^{-9}	$\Omega m^{\circ}C^{-2}$	[5]	α_3	7.0×10^{-10}	$\Omega m^{\circ}C^{-3}$	[5]
α_4	-3.7×10^{-11}	$\Omega m^{\circ}C^{-4}$	[5]	α_5	1.2×10^{-12}	$\Omega m^{\circ}C^{-5}$	[5]
α_6	-2.5×10^{-14}	$\Omega m^{\circ}C^{-6}$	[5]	α_7	3.2×10^{-16}	$\Omega m^{\circ}C^{-7}$	[5]
α_8	-2.2×10^{-18}	$\Omega m^{\circ}C^{-8}$	[5]	α_9	6.7×10^{-21}	$\Omega m^{\circ}C^{-9}$	[5]

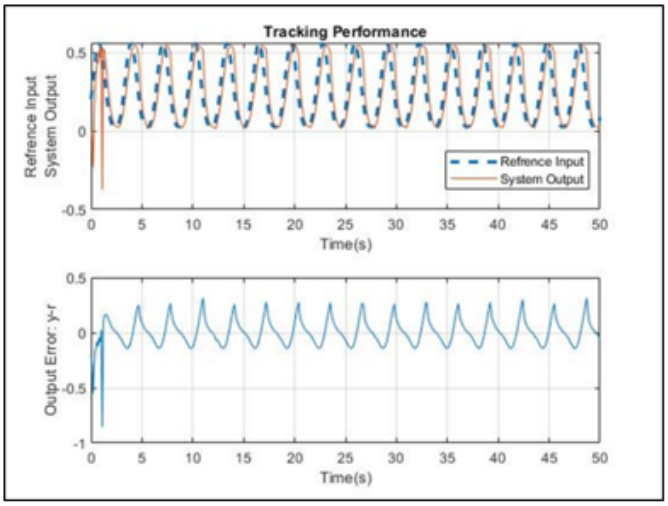

Figure 7: Simulation of system tracking under high frequency input with Q_2 and R_2 weighting matrix

References

[1] H.T. Banks, B.M. Lewis and H.T. Tran, *Nonlinear feedback controllers and compensators: a state-dependent Riccati equation approach*, Comput. Optim. Appl. **37** (2007), no. 2, 177–218.

[2] Y. Batmani and H. Khaloozadeh, *Optimal chemotherapy in cancer treatment: state dependent Riccati equation control and extended Kalman filter*, Optim. Control Appl. Meth. **34** (2013), no. 5, 562–577.

[3] Z. Bo and D.C. Lagoudas, *Thermomechanical modeling of polycrystalline SMAs under cyclic loading, Part I: theoretical derivations*, Int. J. Eng. Sci. 37 (1990), no. 9, 1089–1140.

[4] V. Brailovski, F. Trochu and G. Daigneault, *Temporal characteristics of shape memory linear actuators and their application to circuit breakers*, Mater. Des. **17** (1996), no. 3, 151–158.

[5] S.M. Dutta and F.H. Ghorbel, *Differential hysteresis modeling of a shape memory alloy wire actuator*, IEEE/ASME Trans. Mechatronics **10** (2005), no. 2, 189–197.

[6] M.H. Elahinia and H. Ashrafiuon, *Nonlinear control of a shape memory alloy actuated manipulator*, J. Vib. Acoust **124** (2002), no. 4.

[7] D. Hughes and J.T. Wen, *Preisach modeling of piezoceramic and shape memory alloy hysteresis*, Smart Mater. Struct. **6** (1997), no. 3, 287–300.

[8] N. Kha and K. Ahn, *Position control of shape memory alloy actuators by using self Tuning fuzzy PID controller*, 1ST IEEE Conf. Ind. Electron. Appl., 2006, pp. 1-–5.

[9] N.B. Kha, K.K. Ahn, Y.J. Yum, S.M.M. Rahman and J.H. Son, *Internal model control for shape memory alloy actuators using fuzzy based preisach model*, Int. Conf. Mechatron. Autom., 2007, pp. 2575–2580.

[10] J. Li and H. Tian, *Position control of SMA actuator based on inverse empirical model and SMC-RBF compensation*, Mech. Syst. Signal Process. **108** (2018), 203–215.

[11] N. Ma and G. Song, *Control of shape memory alloy actuator using pulse width modulation*, Smart Mater. Struct. **12** (2003), no. 5, 712–719.

[12] D.R. Madill and D. Wang, *Modeling and L/sub 2/-stability of a shape memory alloy position control system*, IEEE Trans. Control Syst. Technol. **6** (1998), no. 4, 473–481.

[13] J. Mohd Jani, M. Leary, A. Subic and M.A. Gibson, *A review of shape memory alloy research, applications and opportunities*, Mater. Des. **56** (2014), 1078–1113.

[14] A. Pai, M. Riepold and A. Trächtler, *Model-based precision position and force control of SMA actuators with a clamping application*, Mechatronics **50** (2018), 303–320.

[15] H. Pang and T. Liu, *Optimal control for a class of affine nonlinear systems based on SDRE and Improved Newton Method*, 24th Chinese Control and Decision Conference (CCDC), 2012, no. 1, pp. 2425–2429.

[16] N.T. Tai and K.K. Ahn, *Output feedback direct adaptive controller for a SMA actuator with a kalman filter*, IEEE Trans. Control Syst. Technol. **20** (2012), no. 4, 1081–1091.

[17] A. Villoslada et al., *Position control of a shape memory alloy actuator using a four-term bilinear PID controller*, Sensors Actuators A Phys. **236** (2015), 257–272.

[18] G. Webb, L. Wilson, D. Lagoudas and O. Rediniotis, *Adaptive control of shape memory alloy actuators for underwater biomimetic applications*, AIAA J. **38** (2000), no. 2, 325–334.

[19] G.V. Webb, D.C. Lagoudas and A.J. Kurdila, *Hysteresis modeling of SMA actuators for control applications*, J. Intell. Mater. Syst. Struct. **9** (1998), no. 6, 432–448.

[20] M.R. Zakerzadeh and H. Sayyaadi, *Precise position control of shape memory alloy actuator using inverse hysteresis model and model reference adaptive control system*, Mechatronics **23** (2013), no. 8, 1150–1162.